"The Magnetized Interstellar Medium"
8–12 September 2003, Antalya, Turkey
Eds.: B. Uyanıker, W. Reich & R. Wielebinski

Magnetic Fields in Spiral Galaxies

Marita Krause

Max-Planck-Institut für Radioastronomie, Auf dem Hügel 69, 53121 Bonn, Germany

Abstract. Large-scale regular magnetic fields with a spiral pattern exist in grand-design spirals, flocculent and even irregular galaxies. The regular field in spirals is aligned with the optical spiral arms but is usually strongest in the interarm regions, sometimes forming 'magnetic arms'. The strongest total field is found in the optical arms, but is mainly irregular. The large-scale regular field is best explained by some kind of dynamo action. Only a few galaxies show a dominant axisymmetric field pattern, most field structures seem to be a superposition of different dynamo modes or trace local effects related to density waves, bars or shocks. Observations of edge-on galaxies show that the regular magnetic fields are mainly parallel to the disk except in some galaxies with strong star formation and strong galactic winds as e.g. NGC 4631

.

1 Introduction or how to observe magnetic fields

In contrast to Galactic observations, in external galaxies we look as a whole at the spiral structure and the magnetic field structure. Further we integrate the emission along the line of sight through the galaxy. This has the advantage that we can assume one single distance for the emission as the distance to the galaxy (which is known) is large compared to the line of sight through it. In the first decades of observations of magnetic fields in external galaxies we were mainly interested in identifying the global structure of the magnetic field. Meanwhile receivers became significantly more sensitive, which allowed us to observe external galaxies at higher linear resolution with sufficient signal-to-noise ratio. Hence we can observe magnetic fields in more detail and compare them with other constituents of the galaxies like Hα, star-forming regions, dust lanes, density waves, local shocks, etc.

However, when we compare the results from external galaxies with the Galaxy we should be aware that for the former the spatial resolution usually is still worse than about (a few) 100 pc and that we integrate the emission along the line of sight, whereas in the Galaxy we observe the local structure around the solar system with a very high linear resolution. This is difficult to separate from the more distant structure.

Radio observations of the continuum emission are the best way to study magnetic fields in galaxies. The total intensity of the synchrotron emission gives the strength of the total magnetic field. The linearly polarized intensity reveals the strength and the structure of the resolved regular field in the sky plane (i.e. perpendicular to the line of sight). However, the observed polarization vectors suffer Faraday rotation and depolarization (i.e. a decrease of the degree of linear polarization when compared to the intrinsic one) on the way from the radiation's origin to us. Correction for Faraday rotation is possible with observations at two – or better more – wavelengths by determining the rotation measure RM (being proportional to $\int n_{\rm e} B_{\|}\, dl$). The rotation measure itself is proportional to the magnetic field strength parallel to the line of sight, and its sign gives the direction of this magnetic field component. The field strength of both components, parallel and perpendicular to the line of sight, together with the information of the intrinsic polarization vectors enables us in principle to perform a 'tomography' of the magnetic field.

2 Faraday rotation and depolarization effects

Figure 1 gives an example of observations of M51 at four different wavelengths, all smoothed to the same linear resolution of $75''$ HPBW. The vectors are rotated by $90°$ but not corrected for Faraday rotation. The figure illustrates nicely the wavelength-dependent effects of Faraday rotation and depolarization: the observed vectors at $\lambda 2.8$ cm and $\lambda 6$ cm are mainly parallel to the optical spiral arms as expected in spiral galaxies (see below), since Faraday rotation is small at centimeter wavelengths. However, the pattern looks very different at $\lambda 18/20$ cm where Faraday rotation is expected to be strong. Further, we see a region in the northeastern part of M51 with complete depolarization.

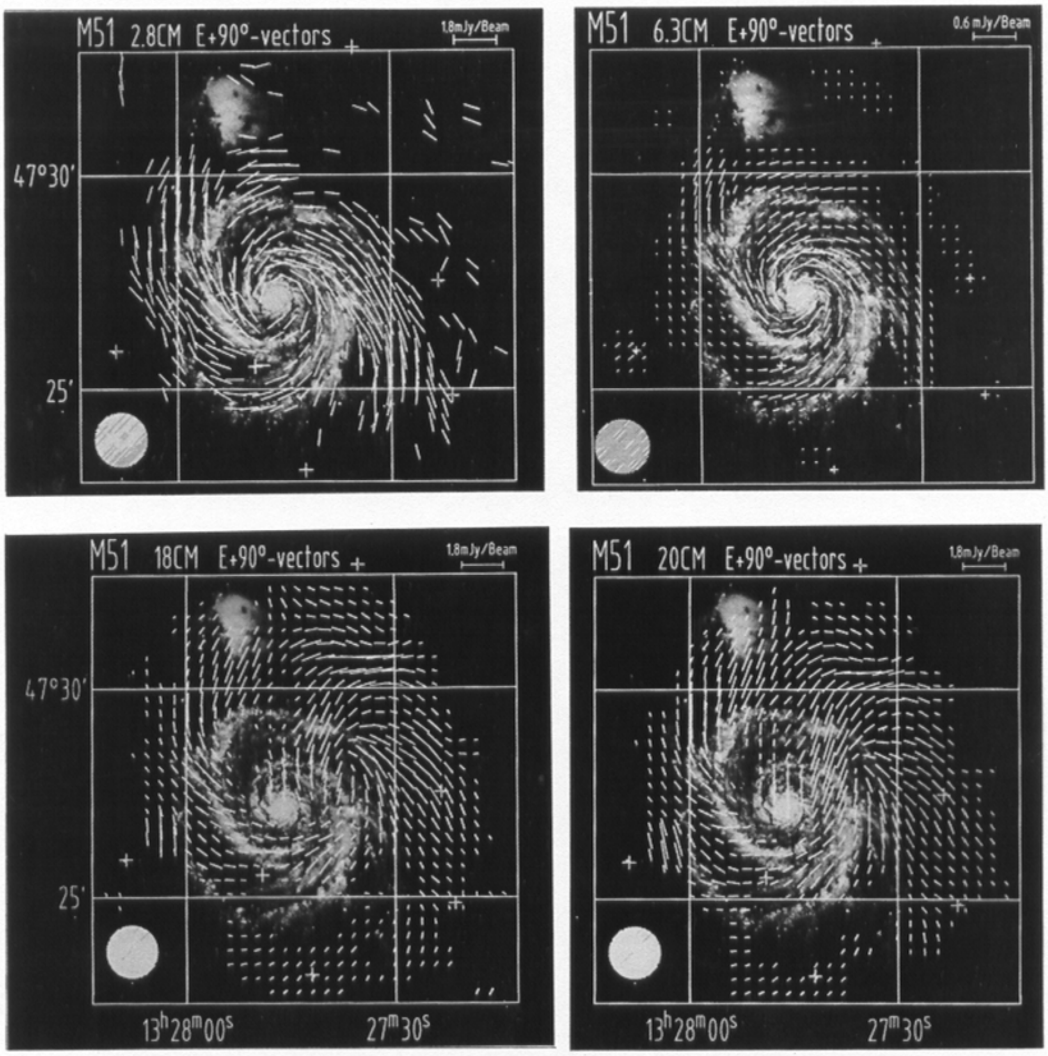

Fig. 1. Maps of the E-vectors rotated by 90° of M51 observed at $\lambda\lambda 2.8$ cm, 6.2 cm, 18.0 cm, and 20.5 cm. The length of the vectors is proportional to the polarized intensity. They are shown superimposed onto an optical picture (Lick Observatory) (Berkhuijsen et al. 1997).

After substraction of the thermal fraction of the emission we distinguish between wavelength-independent and wavelength-dependent depolarization. The difference in depolarization at different wavelengths in maps with the same linear resolution should be purely wavelength-dependent where two different wavelength-dependent depolarization effects are important to consider: the differential Faraday rotation, Faraday dispersion, and a RM gradient within the beam (Burn 1966; Sokoloff et al. 1998). The latter effect allowed the detection of a magneto-ionic screen above the synchrotron disk of M31 (Fletcher et al. 2004). Faraday dispersion is due to turbulent magnetic fields within the source and between the source and us, whereas differential Faraday rotation depends on the regular magnetic field within the emitting source. All three effects have a strong wavelength dependence. The depolarization by differential Faraday rotation has several maxima and minima as shown e.g. in Fig. 1

in Sokoloff et al. (1998) leading to a complete depolarization at $\lambda 20$ cm already at RM $\approx 40\,\mathrm{rad/m^2}$, with weaker depolarization for higher RMs. Such an effect has first been detected in small isolated areas in M51 (Horellou et al. 1992). At $\lambda 6$ cm the depolarization is much weaker, going smoothly to zero at RM $\approx 400\,\mathrm{rad/m^2}$ (the first zero point is at RM $= \pi/(2 \cdot \lambda^2)$).

Hence, the galaxies may not be transparent in linear polarization at decimeter wavelengths so that we may observe just an upper layer of the whole disk. At centimeter wavelengths we do not expect complete depolarization even in galaxies viewed edge-on, i.e. centimeter wavelengths are best suited to trace the magnetic field structure.

3 Magnetic field strength

The total magnetic field strength in a galaxy can be estimated from the nonthermal radio emission under the assumption of equipartition between the energies of the magnetic field and the relativistic particles (the so-called **energy equipartition**). The degree of linear polarization and some assumptions about the geometry give the strength of the magnetic field that has a uniform direction within the beam. The estimates are based on the formulae given by e.g. Pacholczyk (1970) and Segalowitz et al. (1976), and are described e.g. by Krause et al. (1984) and Beck (1991). In our Galaxy the equipartition assumption was verified with independent information about the local cosmic-ray energy density from in-situ measurements and about their radial distribution from γ-ray observations. Combination with the nonthermal radio emission gives almost the same local strength of the total magnetic field of $6\,\mu$G (Strong et al. 2000) as that derived from energy equipartition (Berkhuijsen, in Beck 2001).

The magnetic field in spiral galaxies has been found to be mainly parallel to the galactic disk and to show a spiral pattern similar to that of the optical spiral arms. The total magnetic field strength is generally highest at the positions of the optical spiral arms, whereas the highest regular fields are found *offset* from the optical arms and in the interarm region.

The mean equipartition value for the total magnetic field strength for a sample of 74 spiral galaxies observed by Niklas (1995) is on average $9\,\mu$G with a standard deviation of $3\,\mu$G. It can however reach higher values *within* spiral arm regions of about $20\,\mu$G in NGC 6946 (Beck 1991) and even $25\,\mu$G in the prominent spiral arms of M51 (Fletcher et al., in prep.). Strongly interacting galaxies or galaxies with strong central radio emission tend to have generally stronger total magnetic fields.

The strengths of the *regular* fields in spiral galaxies can either be estimated from the degree of linear polarization and the equipartition assumption or from the observed rotation measure RM. There seems to be a systematic bias in both methods (Beck et al. 2003): the regular field strength derived from the RM can be e.g. underestimated when the thermal electron density and the total magnetic field strength are locally anticorrelated *or* overestimated if they are correlated. On the other hand, the calculation from the degree of linear polarization may overestimate the regular field strength if the CR energy density and the total magnetic field strength are correlated as implied by the assumption of energy equipartition.

Notwithstanding this possible bias, the strength of the regular magnetic fields in spiral galaxies (observed with a spatial resolution of a few 100 pc) is typically 1–5 μG. Especially strong regular fields are found in the *interarm* regions of NGC 6946 of about $10\,\mu$G (Beck & Hoernes 1996) and $\simeq 15\,\mu$G at the inner edge of the inner spiral arm in M51 (Fletcher et al., in prep.) as estimated from the degree of polarization and the equipartition assumption.

4 Regular magnetic fields and dynamo action

The large-scale magnetic field is generally thought to be amplified and maintained by the action of a mean-field dynamo. According to the mean-field dynamo theory (e.g. Ruzmaikin et al. 1988; Wielebinski & F. Krause 1993; Beck et al. 1996; Lesch & Chiba 1997) the structure of the large-scale field is also given by the dynamo action. It is generally of spiral shape with different azimuthal field directions and symmetries. The mode that can be excited most easily is the axisymmetric mode (**ASS**) followed by higher modes such as the bisymmetric (**BSS**), etc. The field configurations can be either symmetric (quadrupole type) or asymmetric (dipole type) with respect to the galactic plane.

According to the dynamo theory the pitch angle of the magnetic field spiral is determined by the dynamo numbers, not by the pitch angle of the gaseous spiral arms.

ASS and BSS field configurations can be distinguished observationally by analyzing the rotation measures or – more sophisticated – by analyzing directly the observed polarization vectors at different wavelengths (as has been described e.g. in Sokoloff et al. (1992) and Berkhuijsen et al. (1997)). It has been found that only M31 and IC342 show clear ASS fields in the disks (Beck 1982; Fletcher et al. 2004; Krause et al. 1989a), whereas many other galaxies seem to have a superposition of different modes.

A special case is M81 as it has a *dominating* BSS field (Krause et al. 1998b; Sokoloff et al. 1992). The dominance of the BSS field structure requires an additional physical mechanism to be invoked that can occur only in rare cases. For M81 a three-dimensional, nonlinear dynamo model has been developed including the disturbed velocity field due to the encounter with its companion NGC 3077 (Moss et al. 1993) or alternatively, parametric resonance with the spiral density wave as has been proposed by Chiba & Tosa (1990) and investigated numerically by Moss (1996).

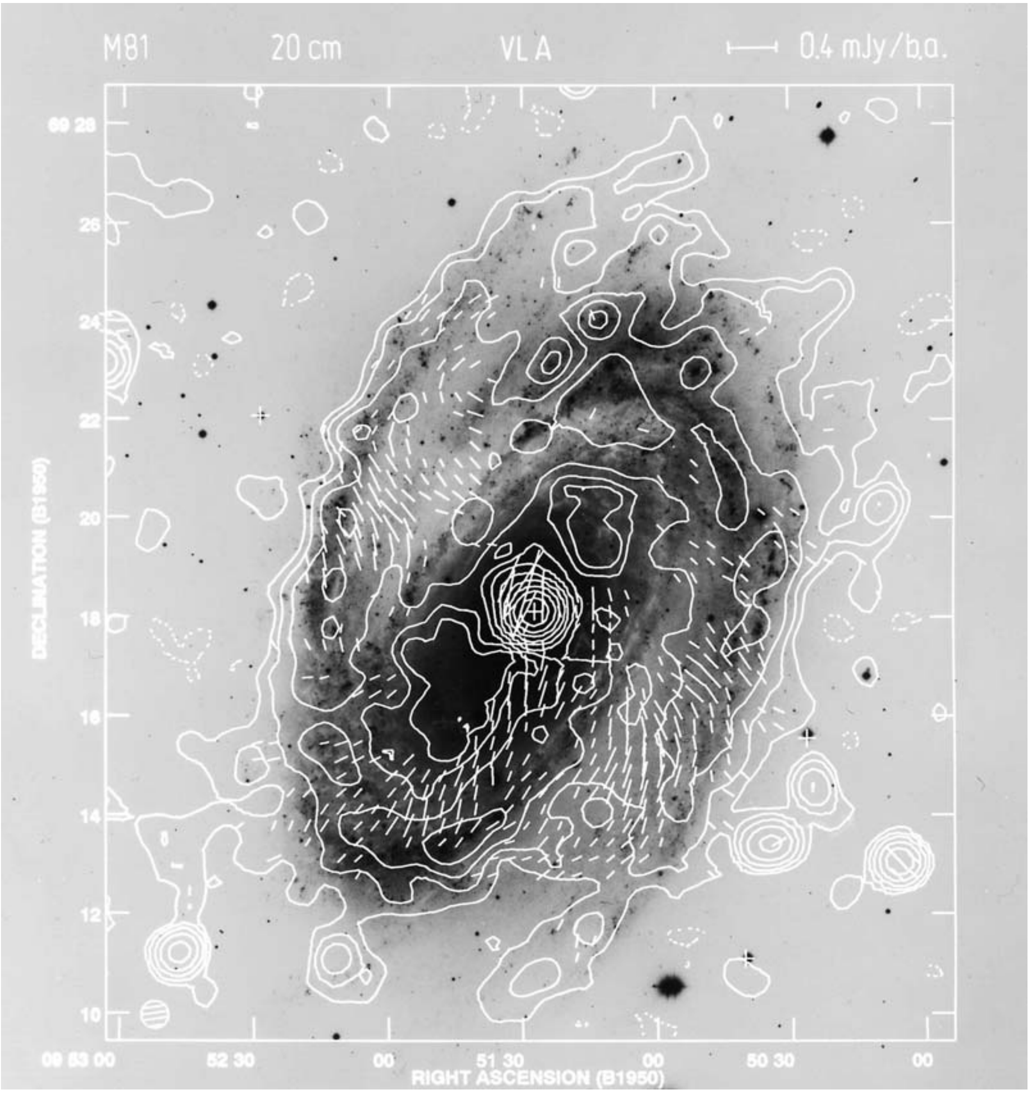

Fig. 2. Total Intensity map at λ20 cm as observed with the VLA in C and D array with an angular resolution of 33″. The orientation of the vectors gives the observed E-vectors, their lengths are proportional to the polarized intensity. They are shown superimposed onto an optical photograph (Palomar plate).

Most other spiral galaxies observed so far indicate a mixture of magnetic modes. The analysis of the observations at all four frequencies of M51 (Fig. 1) even revealed two different magnetic-field configurations for the disk and the halo respectively (Berkhuijsen et al. 1997).

It is clear that such a global description of the regular magnetic field cannot describe local effects that become more and more visible with increasing linear resolution of the observations. Further, in grand-design galaxies the magnetic field lines often follow the dust lanes. In M51 e.g. one dust lane in the eastern part crosses the optical spiral arm, so does the regular magnetic field (visible in Fig. 1 at in the short wavelengths observations).

5 Magnetic fields at higher spatial resolution

The regular magnetic field in spiral galaxies is usually strongest in the region between the optical spiral arms and fills the whole interarm region like e.g. in M81 (see Fig. 2). However, some galaxies host so-called *magnetic arms*. Long, highly polarized features disconnected from the optical spiral arms were first discovered in IC342 (Krause et al. 1989a; Krause 1993). Two symmetric so-called 'magnetic arms' in the interarm region, parallel to but isolated from the optical spiral arms, were found in NGC 6946 (Beck & Hoernes 1996) and are shown in Fig. 3. Their width is less than 1 kpc, hence they do not fill the whole interarm region. Magnetic arms have also been found in NGC 2997 (Han et al. 1999) and M83 (Beck, Ehle & Sukumar, in prep.).

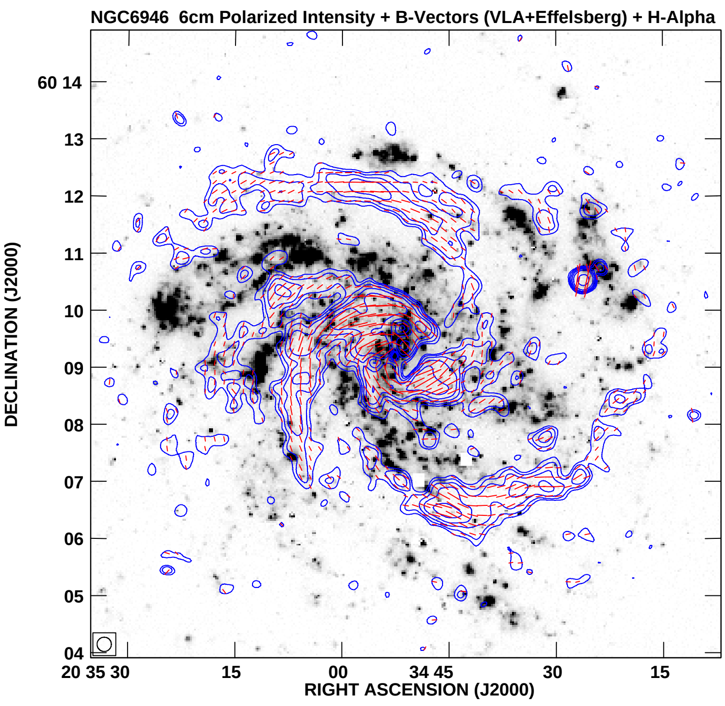

Fig. 3. Polarized radio emission and B-vectors of the spiral galaxy NGC 6946 at $\lambda 6$ cm, combined from observations with the VLA and Effelsberg telescopes. The angular resolution is $15''$. The radio image is overlaid onto an Hα image (Beck 2001).

Several models have been developed to explain these magnetic arms. Slow MHD waves have been proposed by Fan & Lou (1996) and Lou & Fan (1998) to explain the generation of magnetic arms shifted with respect to the optical spiral arms. These MHD waves occur only in an almost rigidly rotating disk. However, all galaxies with magnetic arms are found to rotate differentially beyond 1–2 kpc from the center, different to older measurements with lower angular resolution. Han et al. (1999) found some correlation between the magnetic arms and interarm gas features generated at the 4:1 resonances in numerical models of Patsis et al. (1997).

In the framework of dynamo theory the generation of magnetic arms can be described if one assumes that the turbulent velocity of the gas is higher in the optical arms (Moss 1998; Shukurov 1998), or that turbulent diffusion is larger in the arms (Rohde et al. 1999). Both effects reduce the dynamo number in the spiral arms when compared to the interarm regions and hence allow generation of regular magnetic field preferentially in the interarm region.

Recent observations of M51 at λ6cm with $8''$ HPBW (corresponding to about 400 pc) have been obtained with the VLA and combined with Effelsberg data at the same wavelength in order to get a high-resolution map that is sensitive also to the faint extended emission (Fletcher et al., in prep.). The inner part of this map up to a radius of 4 kpc of M51 is shown in Fig. 4. The total intensity and hence the total magnetic field is strongest on top of the dust lanes, whereas the polarized emission (and the regular magnetic field) is strongest just upstream of the dust lanes but fills the interarm region. These are strong indications that both dynamo action and shock compression produce a large-scale magnetic field in M51.

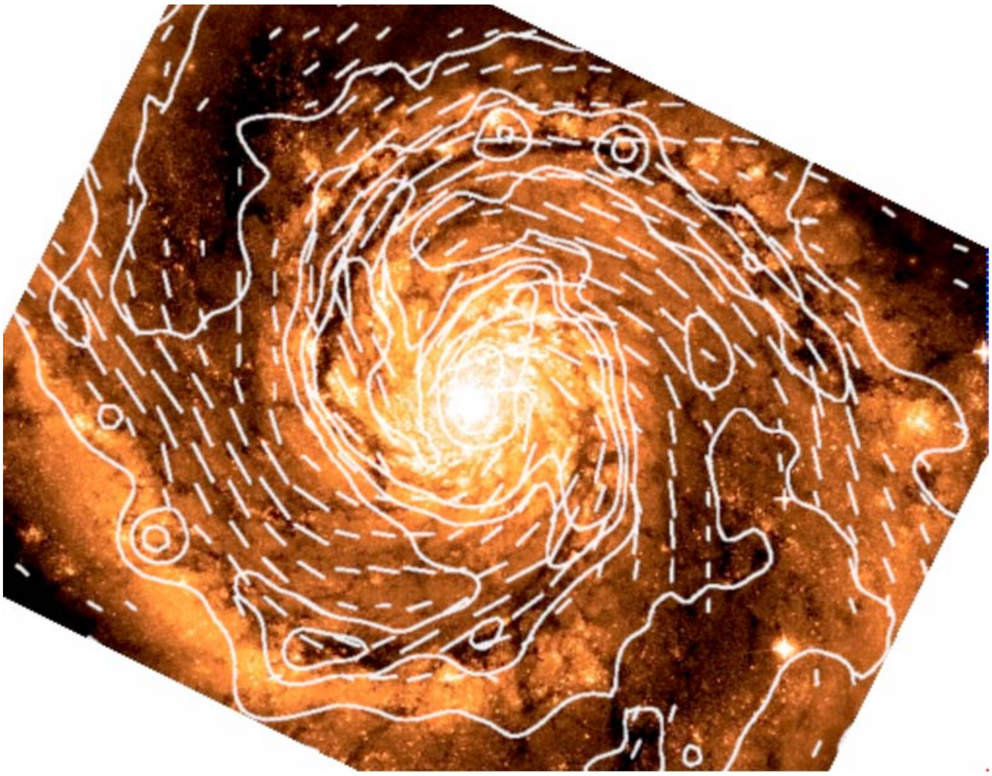

Fig. 4. Total intensity map at λ6 cm observed with the VLA in C and D array and combined with Effelsberg 100-m observations at the same wavelength. The angular resolution of the combined map is $8''$. The orientation of the vectors gives the observed E-vectors rotated by $90°$, their lengths are proportional to the polarized intensity. They are shown superimposed onto the NASA Hubble Heritage image (STScI/AURA) (Fletcher et al., in prep.).

6 Flocculent and irregular galaxies

Regular magnetic fields have also been detected in flocculent galaxies like M33 (Buczilowski & Beck 1991) and NGC 4414 (Soida et al. 2002). These are galaxies with a patchy spiral structure without signs of the action of density waves. The mean degree of polarization (corrected for different angular resolution) is similar between flocculent and grand-design galaxies (Knapik et al. 2000). As expected from classical $\alpha - \Omega$ dynamo models the dynamo works well without the assistance of density waves.

Even in a dwarf irregular galaxy with weak rotation and non-systematic gas motion like NGC 4449 a large-scale (partly spiral) regular magnetic field has been observed (Chyzy et al. 2000). The strength of the regular field reaches $7\,\mu$G and that of the total field $14\,\mu$G, which is high even in comparison with fields strengths of radio-bright spirals. Hence, the magnetic field energy in irregulars might be important for the dynamics of the interstellar medium.

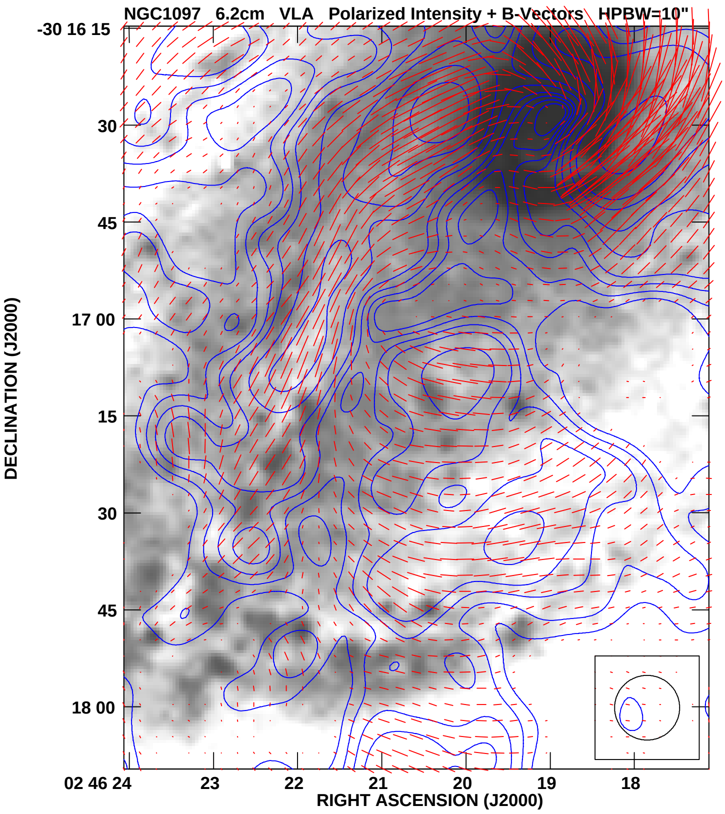

Fig. 5. The total intensity (contours) of the continuum emission at $\lambda 6.2$ cm observed with the VLA in the southern part of NGHC 1097 (the galactic centre is at top right). The E-vectors are rotated by $90°$, still uncorrected for Faraday rotation. The angular resolution is $10''$ (Moss et al. 2001).

The absence of ordered differential rotation requires a different kind of dynamo action in NGC 4449. A fast field amplification is predicted by a dynamo e.g. driven by magnetic buoyancy and sheared Parker instabilities (e.g. Moss et al. 1999; Hanasz & Lesch 1998, 2000) or without any α-effect at all (Blackman 1998).

7 Barred galaxies, shocked areas, and merging galaxies

A sample of 20 barred galaxies has been observed extensively in total power and linear polarization (Beck et al. 2002). They found that the total radio emission (and hence the total magnetic field) is strongest along the bar and correlates with the bar *length*. The regular magnetic field is enhanced *upstream* of the shock fronts in the bar. The upstream field lines are at large angle to the bar, but turn smoothly towards the bar orientation about 1 kpc upstream from the dust lanes as observed in NGC 1097 (Moss et al. 2001) without any indication for shock compression. This is shown in Fig. 5 for the southern part of the bar in NGC 1097. Similar smooth turns have been observed in NGC 1365, NGC 1672, and NGC 7552 (Beck et al. 2002). For NGC 1097 the observed regular magnetic field can be well reproduced by using a mean-field dynamo model in which the turbulent diffusivity is enhanced in the dust lanes and near the circumnuclear ring (Moss et al. 2001).

Indications for a compression of the galactic magnetic field – possibly by gas tidally stripped during an interaction with a neighbouring galaxy – have been observed in NGC 3627 (Soida et al. 2001) where the observed regular field apparently crosses the dust lanes at a large angle in the east. Another example for such a compression is the wind-swept galaxy NGC 4254 (Soida et al. 1996).

The mean total magnetic field strength in the merging pair of galaxies NGC 4038/39 (the Antennae) is about two times stronger than in normal spirals, but the degree of field regularity is unusually low. This implies the destruction of regular field in regions of strong star formation due to the interaction. Away from star-forming regions the magnetic field shows a coherent polarized structure with a strong regular component of $10\,\mu$G (Chyzy & Beck 2004).

8 Edge-on galaxies and vertical fields

Several galaxies seen edge-on have been observed in radio continuum and polarization. Most of them have regular magnetic fields that are parallel to the galactic disks (e.g. Dumke et al. 1995).

The apparent disk thicknesses vary quite a lot among the galaxies with plane-parallel field as do their intensities. Interferometer observations of edge-on galaxies have to be combined with single-dish observations in order to correct for the missing zero-spacings before the scale heights of the emission perpendicular to the disk (in z-direction) can be determined. Emission in the z-direction can best be fitted with two exponential functions, whose scale heights are about *equal* for all four galaxies with plane-parallel fields that have been analyzed so far, namely NGC 891, NGC 3628, NGC 4565, NGC 5907 (Dumke & Krause 1998; Dumke et al. 2000). The scale height for the thin disk is $\simeq 300$ pc and that of the thick disk/halo is $\simeq 1.8$ kpc for these galaxies, independent of the star-forming activity and interaction state.

Even the Sombrero galaxy M104, known for its huge bulge, and the strong and active spiral NGC 253 have a dominant plane-parallel magnetic field (Krause & Wielebinski, in prep.; Beck et al. 1994).

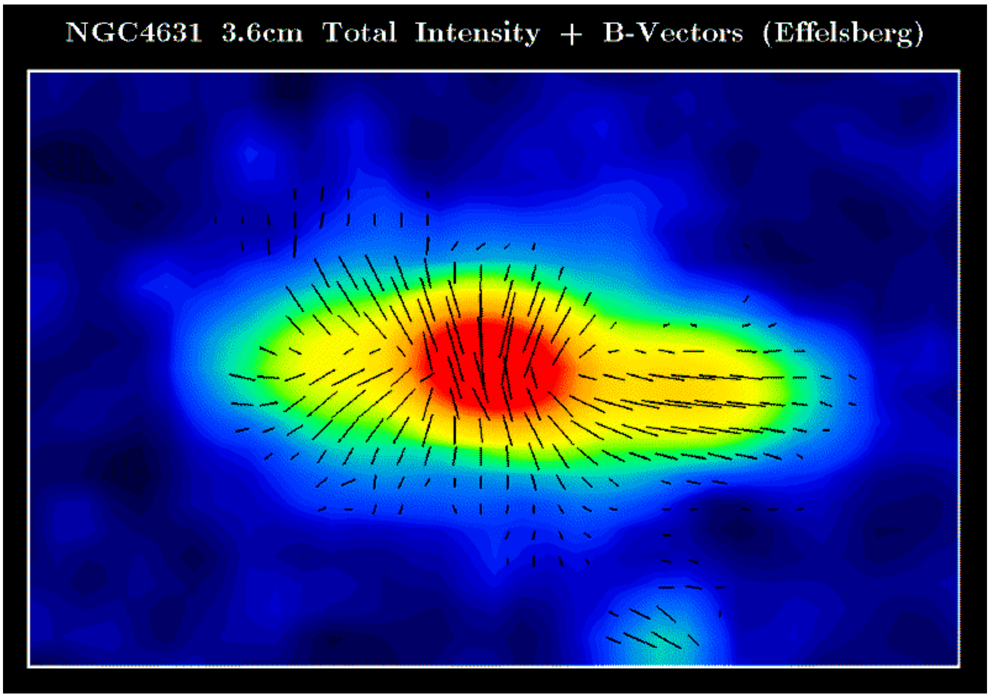

Fig. 6. Contour map of NGC 4631 at λ3.6 cm as observed with the Effelsberg 100-m telescope. The angular resolution is 85″ HPBW. The vectors give the orientation of the intrinsic regular field in the plane of the sky. Their lengths are proportional to the polarized intensity.

Some galaxies are found with regular vertical fields like the starburst galaxy M82 (Reuter et al. 1994) and the spiral NGC 4631 (Golla & Hummel 1994). Also NGC 4217 (M. Urbanik, private comm.), NGC 4666 (Dahlem et al. 1997), and NGC 5775 (Tüllmann et al. 2000) may contain regular vertical fields.

λ3.6 cm observations of NGC 4631 obtained with the Effelsberg 100-m telescope are presented in Fig. 6. Faraday rotation could be determined between this wavelength and λ6.2 cm observations with the VLA and revealed $-300\,\mathrm{rad/m^2} < \mathrm{RM} < 300\,\mathrm{rad/m^2}$. The vectors shown in Fig. 6 give the intrinsic magnetic field orientation. NGC 4631 has a large-scale vertical magnetic field in the central 7 kpc. Outside this radius the field is plane parallel in the western half but still has vertical field components in the eastern half. The RM does not show a typical symmetric pattern as expected from a dipole or quadrupole field. Hence we conclude that the vertical field is rather wind-driven and related to the high star-forming activity in this galaxy. The exponential scale heights for NGC 4631 are about 50% larger than those found for galaxies with plane-parallel fields which may also be related to the galactic winds and vertical fields.

9 Outlook

Much has already been learned about the magnetic field strengths and structure – on scales from several kpc down to a few 100 pc in external galaxies and on pc to sub-pc scales in our Galaxy. However, we are still limited by sensitivity at the required resolution to fill the gap between these scales by observing external galaxies. The extended VLA, the GMRT for lower frequencies, and especially the Square Kilometer Array (SKA) will provide a great opportunity to fill this gap and reveal the full wealth of magnetic fields in galaxies.

References

Beck, R. (1982) *Astron. Astrophys.* **106**, 121.
Beck, R. (1991) *Astron. Astrophys.* **251**, 15.
Beck, R. (2001) *Space Science Review* **99**, 243.
Beck, R., Hoernes, P. (1996) *Nature* **379**, 47.
Beck, R., Carilli, C.L., Holdaway, M.A., Klein, U. (1994) *Astron. Astrophys.* **292**, 409.
Beck, R., Brandenburg, A., Moss, D., Shukurov, A., Sokoloff, D. (1996) *Annnu. Rev. Astron. Astrophys.* **34**, 155.
Beck, R., Shoutenkov, V., Ehle, M., Harnett, J. I., Haynes, R. F., Shukurov, A., Sokoloff, D. D., Thierbach, M. (2002) *Astron. Astrophys.* **391**, 83.
Beck, R., Shukurov, A., Sokoloff, D., Wielebinski, R. (2003) *Astron. Astrophys.* **411**, 99.
Berkhuijsen, E.M., Horellou, C., Krause, M., Neininger, N., Poezd, A.D., Shukurov, A., Sokoloff, D. (1997) *Astron. Astrophys.* **318**, 700.
Blackman, E.G. (1998) *Astrophys. J.* **496**, L17.
Buczilowski, U.R., Beck, R. (1991) *Astron. Astrophys.* **241**, 47.
Burn, B.J. (1966) *Mon. Not. R. Astron. Soc.* **133**, 67.
Chiba, M., Tosa, M. (1990) *Mon. Not. R. Astron. Soc.* **244**, 714.
Chyzy, K.T., Beck R. (2004) *Astron. Astrophys.*, in press.
Chyzy, K.T., Beck, R., Kohle, S., Klein, U., Urbanik, U. (2000) *Astron. Astrophys.* **355**, 128.
Combes, F. (1991) *Annnu. Rev. Astron. Astrophys.* **29**, 195.
Dahlem, M., Petr, M.G., Lehnert, M.D., Heckman, T.M., Ehle, M. (1997) *Astron. Astrophys.* **320**, 731.
Dumke, M., Krause, M. (1998) in *The Local Bubble and Beyond*, eds. D. Breitschwerdt, M. Freyberg, J. Trümper, Lecture Notes in Physics, Springer, p. 555.
Dumke, M., Krause M. (2000) *Astron. Astrophys.* **355**, 512.
Dumke, M., Krause, M., Wielebinski, R., Klein, U. (1995) *Astron. Astrophys.* **302**, 691.
Fan, Z., Lou, Y.Q. (1996) *Nature* **383**, 800.
Fletcher, A., Berkhuijsen, E.M., Beck, R., Shukurov, A. (2004) *Astron. Astrophys.*, in press.
Golla, G., Hummel, E. (1994) *Astron. Astrophys.* **284**, 777.
Han, J.L., Beck, R., Ehle, M., Haynes, R.F., Wielebinski, R. (1999) *Astron. Astrophys.* **348**, 40.
Hanasz, M., Lesch, H. (1998) *Astron. Astrophys.* **332**, 77.
Hanasz, M., Lesch, H. (2000) *Astrophys. J.* **543**, 235.
Horellou, C., Beck, R., Berkhuijsen, E.M., Krause, M., Klein, U. (1992) *Astron. Astrophys.* **265**, 417.
Knapik, J., Soida, M., Dettmar, R.-J., Beck, R., Urbanik, M. (2000) *Astron. Astrophys.* **362**, 910.
Krause, M. (1990) in *Galactic and Intergalactic Magnetic Fields*, eds. R. Beck, P.P. Kronberg, R. Wielebinski, Kluwer, p. 187.
Krause, M. (1993) in *The Cosmic Dynamo*, eds. F. Krause et al., Kluwer, p. 305.
Krause, M., Beck, R., Klein U., (1984) *Astron. Astrophys.* **138**, 385.
Krause, M., Hummel, E., Beck, R. (1989a) *Astron. Astrophys.* **217**, 4.
Krause, M., Beck, R., Hummel, E. (1989b) *Astron. Astrophys.* **217**, 17.
Lesch, H., Chiba, M. (1997) *Fund. Cosmic Phys.* **18**, 273.
Lou, Y.Q., Fan, Z. (1998) *Astrophys. J.* **493**, 102.
Moss, D. (1996) *Astron. Astrophys.* **308**, 381.
Moss, D. (1998) *Mon. Not. R. Astron. Soc.* **297**, 860.
Moss, D., Brandenburg, A., Donner, K.J., Thomasson, M. (1993) *Astrophys. J.* **409**, 179.
Moss, D., Shukurov, A., Sokoloff, D. (1999) *Astron. Astrophys.* **343**, 120.
Moss, D., Shukorov, A., Sokoloff, D., Beck, R., Fletcher, A. (2001) *Astron. Astrophys.* **380**, 55.
Niklas, S. (1995) PhD thesis, University of Bonn.
Pacholczyk, A.G. (1970) *Radio Astrophysics*, Freeman.
Patsis, P.A., Grosbøl, P., Hiotelis, N. (1997) *Astron. Astrophys.* **323**, 762.
Reuter, H.-P., Klein, U., Lesch, H., Wielebinski, R., Kronberg P.P. (1994) *Astron. Astrophys.* **282**, 724.

Rohde, R., Beck, R., Elstner, D. (1999) *Astron. Astrophys.* **350**, 423.
Ruzmaikin, A.A., Shukurov, A.M., Sokoloff, D.D. (1988), *Magnetic Fields of Galaxies*, Kluwer.
Segalovitz, A., Shane, W.W., de Bruyn, A.G. (1976) *Nature* **264**, 222.
Shukurov, A. (1998) *Mon. Not. R. Astron. Soc.* **299**, L21.
Soida, M., Urbanik, M., Beck, R. (1996) *Astron. Astrophys.* **312**, 409.
Soida, M., Urbanik, M., Beck, R., Wielebinski, R, Balkowski, C. (2001) *Astron. Astrophys.* **378**, 40.
Soida, M., Beck, R., Urbanik, M., Braine, J. (2002) *Astron. Astrophys.* **394**, 47.
Sokoloff, D., Shukurov, A., Krause, M. (1992) *Astron. Astrophys.* **264**, 396.
Sokoloff, D.D., Bykov, A.A., Shukurov, A., Berkhuijsen, E.M., Beck, R., Poezd, A.D. (1998) *Mon. Not. R. Astron. Soc.* **299**, 189.
Strong, A.W., Moskalenko, I.V., Reimer, O. (2000) *Astrophys. J.* **537**, 763.
Tüllmann, R., Dettmar, R.-J., Soida, M., Urbanik, M., Rossa, J. (2000) *Astron. Astrophys.* **364**, L36.
Wielebinski, R., Krause, F. (1993) *Astron. Astrophys. Rev.* **4**, 449.

"The Magnetized Interstellar Medium"
8–12 September 2003, Antalya, Turkey
Eds.: B. Uyanıker, W. Reich & R. Wielebinski

Magnetic Fields in Galaxies – 3-D Numerical Simulations

Marian Soida and Katarzyna Otmianowska-Mazur

Astronomical Observatory, Jagiellonian University, ul. Orla 171, PL-30-244 Kraków, Poland

Abstract. Results of modeling the magnetic field in a spiral galaxy are presented. Our 3-D MHD simulations (with the ZEUS3D code) use the global velocity field from self-gravitating, N-body sticky-particle simulations. As external working agent, ram pressure was adopted to model interaction with the intracluster medium.
The resulting magnetic field cube was finally used to integrate synchrotron emissivities in I, Q and U Stokes parameters. For comparison with observations, final maps where smoothed with a Gaussian beam.
External interaction – caused by ram pressure – was found to be an efficient mechanism for magnetic field amplification in galaxies.

1 Introduction

There is still a growing number of observations devoted to magnetic field structure in nearby galaxies (see e.g. Beck et al. 1996 and Beck 2000 for reviews). Recent studies of galaxies interacting with the intergalactic medium like NGC 4254 (Soida et al. 1996, Chyży et al. 2002), interacting with other group members like NGC 3627 (Soida et al. 1999 and 2001), or colliding like NGC 4038/39 (Chyży et al. 2003) show completely new phenomena compared to regular spirals. To understand such cases, modeling of a whole galaxy is necessary. Technical limitations force us to focus on some global phenomena only rather than studying every detailed structure.

This contribution presents an attempt to model the magnetic field configuration in a galaxy influenced by an intergalactic wind as it is seen in polarization data achieved for the two Virgo Cluster members NGC 4254 and NGC 4569.

2 The model – information flow

The model is constructed in the following steps, schematically shown in Fig. 1:

i) A 3-dimensional, N-body, sticky-particle code simulating the whole galaxy consisting of 10 000 gas cloud complexes with various masses. Clouds can collide inelastically, fragment and coagulate. An analytically prescribed potential of the bulge and the halo is applied. Ram pressure is added as an additional acceleration of the clouds located at the surface exposed to the intracluster wind (see Vollmer et al. 2001 for details). The wind itself is modeled as the Gaussian impulse of ram pressure (with the maximum at the evolution time $t = 0$).

ii) The 3-D velocity field obtained in the previous step is used in the 3-D MHD code (Zeus3D – Stone & Norman 1992) with a rectangular grid consisting of $171 \times 171 \times 71$ cells (34 kpc × 34 kpc × 20 kpc in size). The induction (dynamo) equation

$$\frac{\partial}{\partial t}\vec{B} = \nabla \times (\vec{v} \times \vec{B}) + \nabla \times (\alpha\ \vec{B}) - \nabla \times (\eta\ \nabla \times \vec{B})$$

is solved. $\vec{B}$ and $\vec{v}$ are the large-scale magnetic induction and the velocity of the gas, α and η are the dynamo coefficients.

We adopted outflow boundary conditions and a toroidal (azimuthal) initial magnetic field configuration 300 Myr before the maximum of interaction (at $t = -300$ Myr).

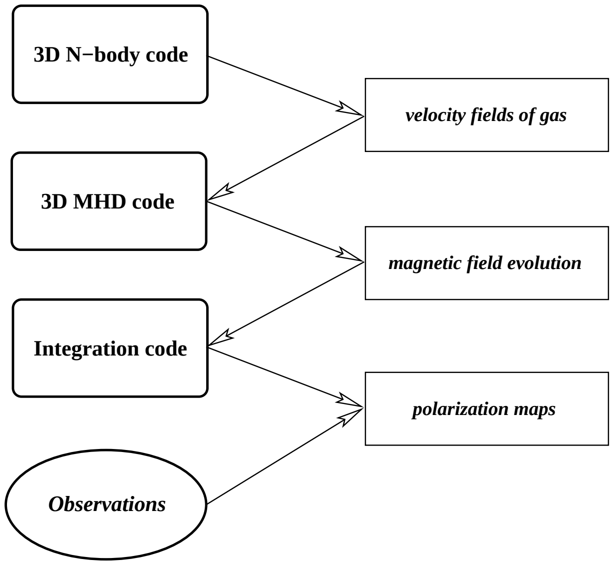

Fig. 1. Information and data flow in modeling of the magnetic field in galaxies

Dynamo coefficients were varied in various experiments, the ones presented in this contribution are $\alpha = 0$ and $\eta = 5 \times 10^{25}\,\mathrm{cm}^2/\mathrm{s}$ (see Otmianowska-Mazur & Vollmer 2003 for more details, and particulary for discussion on the effects of numerical diffusion).

As N-body data are discrete, we have to interpolate (and extrapolate) them into the regular grid. Our own 3-D extension to the "krigging" algorithm (Isaaks & Srivastava 1989) was applied.

iii) The cube of 3-D magnetic field is oriented in space according to the orientation of the modeled galaxy, and the transfer equations of synchrotron emissivities in Stokes I, Q and U parameters are integrated along the line of sight

$$\frac{d}{dl}\begin{pmatrix} I \\ Q \\ U \end{pmatrix} = \begin{pmatrix} \epsilon_I & 0 & 0 \\ p\epsilon_I \cos 2\chi & \cos\Delta & -\sin\Delta \\ p\epsilon_I \sin 2\chi & \sin\Delta & \cos\Delta \end{pmatrix} \begin{pmatrix} I \\ Q \\ U \end{pmatrix}$$

where the synchrotron emissivity

$$\epsilon_I \propto n_{rel} B_\perp^{(\gamma+1)/2}$$

with a relativistic electron spectral index of $\gamma = 2.8$, and the Faraday rotation angle

$$\Delta \propto n_{th} B_\parallel$$

where subscripts $\perp$ and $\parallel$ are used with respect to the line of sight.

The intrinsic degree of synchrotron polarization was assumed to be $p = 75\%$.

Both, thermal and relativistic electron distributions were taken as Gaussians

$$n_{rel|th} \propto \mathrm{e}^{-(\mathrm{R}/\mathrm{R}_0)^2} \mathrm{e}^{-(\mathrm{z}/\mathrm{z}_0)^2}$$

where the radial scale-length R_0 was set to 10 kpc and the scale-height z_0 to 1 kpc for the face-on and edge-on views presented here.

In the results shown here we neglect Faraday effects by setting $n_{th} = 0$.

iv) For direct comparison with radio observations, the model maps of Stokes I, Q and U were convolved with a 2-D Gaussian function with a HPBW of $10''$. The final Q and U maps were combined to obtain maps of polarized intensity and polarization angle (rotated by 90° to show the magnetic vector).

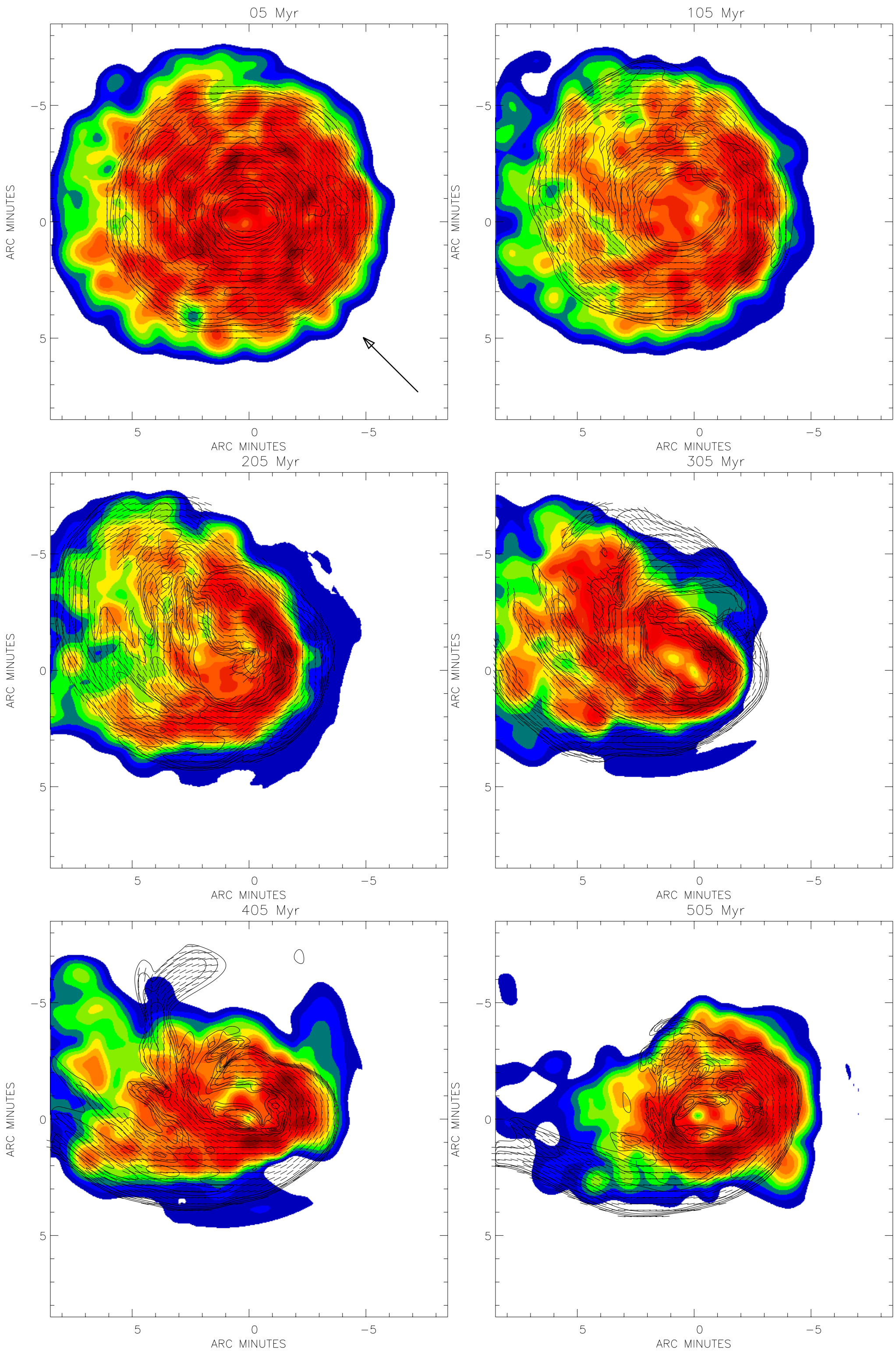

Fig. 2. Face-on view (inclination 30°) of the modeled galaxy. Polarized intensity contours with magnetic vectors overlaid upon the integrated gas density (in logarithmic scale) shown in 100 Myr time steps. The arrow in the first plot indicates the direction of external ram pressure

3 Results and comparison with observations

Figures 2 and 4 show the evolution of polarized emission from a galaxy just after it underwent interaction by an intracluster wind, as seen face-on and edge-on, respectively. Both time sequences differ only in the viewing angle.

3.1 Face-on view

After the compression phase, seen at a time $t = 105\,\mathrm{Myr}$ as more crowded contours of the polarized intensity on the wind side (lower right), the region with compressed magnetic field follows the global galactic rotation, but it apparently rotates with a different speed than the underlying gaseous structures. At a later stage ($t = 405\,\mathrm{Myr}$) this behavior results in a strong magnetic (polarized) arm (sticking out northwards) just *aside* the optical (gaseous) one. One can say that the gaseous arm lies *between* two magnetic ones (in the north-eastern quadrant).

In addition to this structure, at the same evolution time ($t = 405\,\mathrm{Myr}$) the internal part of the southern magnetic arm meets with the northern one, with the magnetic vectors perpendicular to each other. This results in a narrow channel depolarized due to beam depolarization. It is interesting that this feature runs *across* the underlying optical (gaseous) structure.

Both such features have been observed for the first time in the Virgo Cluster member NGC 4254 (Chyży et al. 2001 and Fig. 3).

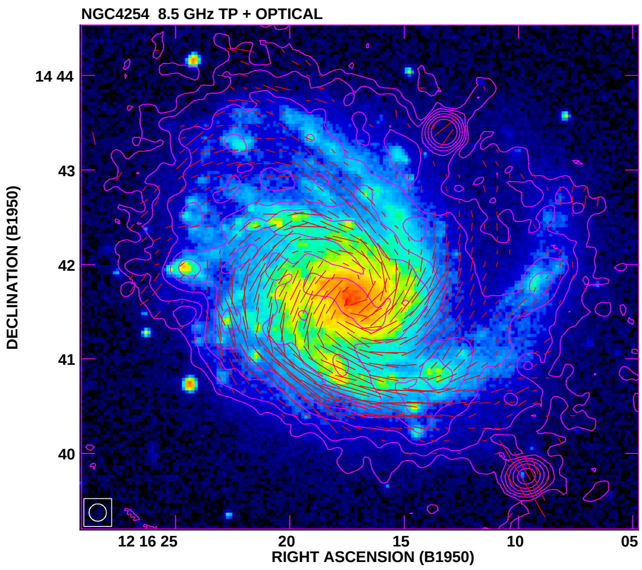

Fig. 3. Optical image of NGC 4254 with superimposed contours of total power emission and magnetic vectors with their length proportional to the polarized intensity

A narrow depolarized channel is seen south-east from the galaxy center (the place where perpendicular magnetic field vectors meet within one beam area). Beside the strong southern magnetic arm (compression area) two other arms are located just between the underlying optical structure – one in the western part of the galaxy (seen already in the low-resolution maps of Soida et al. 1996), the second in the northern part – between the somewhat patchy region looking like two other optical spiral arms.

3.2 Edge-on view

The edge-on view of the presented model shows a mostly plane-parallel magnetic field structure (Fig. 4). As the interacting wind hits the galactic plane with some angle (30°), it ignites vertical gas motions, and in consequence vertical magnetic field structures start to develop. Traces of magnetic

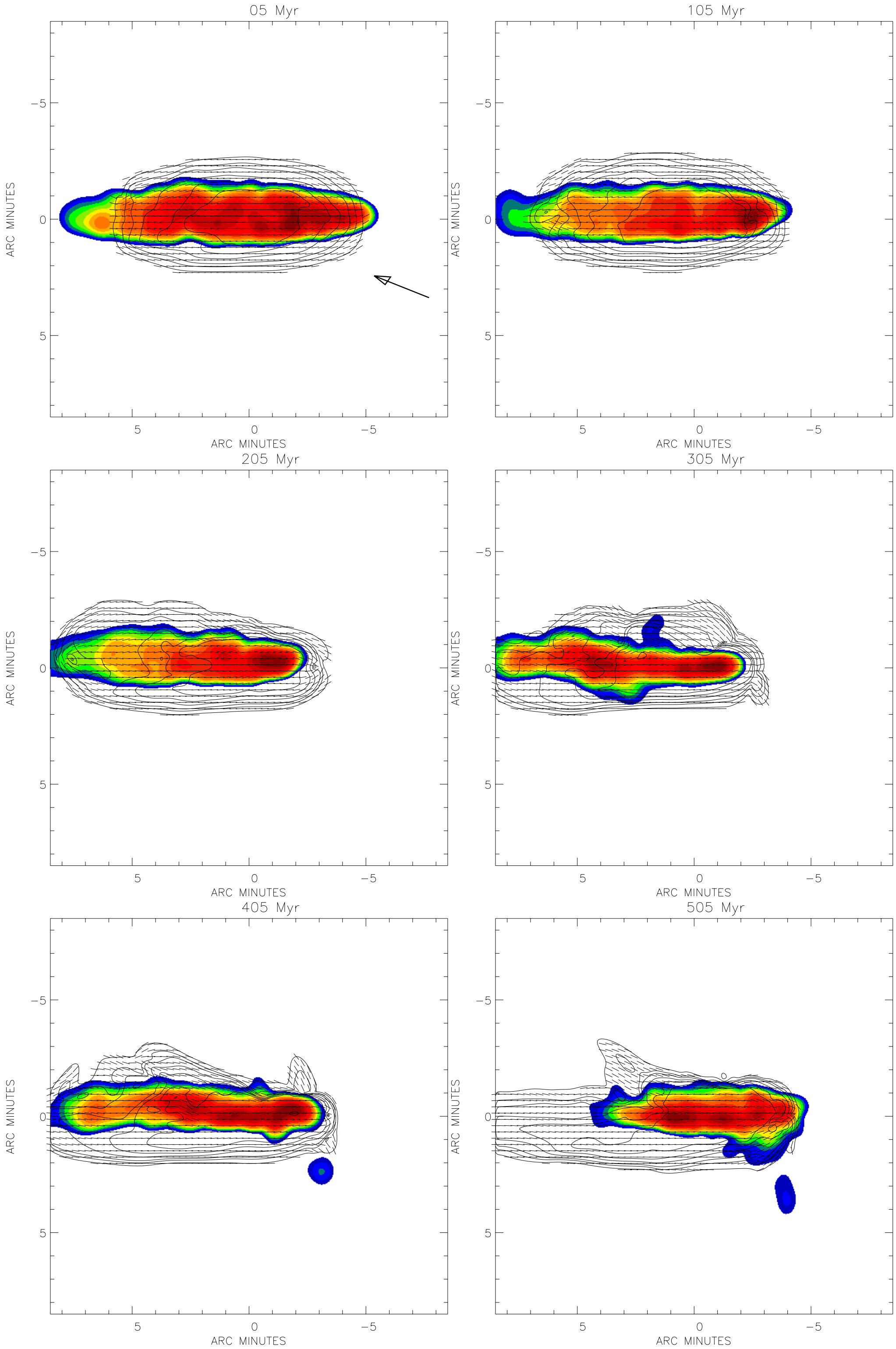

Fig. 4. Edge-on view (inclination of 85°) of the same model as in Fig. 2

loops are visible at an evolution time of $t = 305\,\mathrm{Myr}$. At later stages the footpoints of such loops are visible at both ends of the galactic disk (pointed northwards) as well.

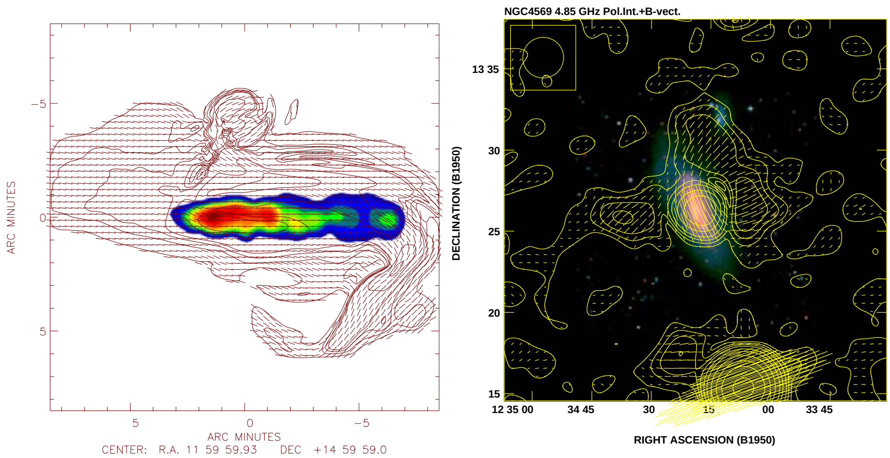

Fig. 5. Modeled galaxy (left) computed with a $z_0 = 10\,\mathrm{kpc}$ scale-height of the relativistic electron distribution and an optical image of NGC 4569 with polarized intensity contours and magnetic vectors (right)

For better visualization of the vertical magnetic field structure the same model was recalculated assuming a very large scale-height of the relativistic electron distribution ($z_0 = 10\,\mathrm{kpc}$). The result is presented in the Fig. 5 (left panel) together with the radio polarization map of another Virgo Cluster member, NGC 4569 (right panel – Chyży, priv. comm.). Some traces of magnetic loops are seen in Fig. 4. The loops are obvious in Fig. 5 and they extend well more than 10 kpc from the modeled galactic disk. In NGC 4569 the loop-like structure is seen on the western side of the galaxy (this is much better seen in higher resolution data obtained very recently with the VLA – Chyży, priv. comm.).

The mechanism of supplying relativistic electrons at more than 10 kpc distance from the galaxy plane (where the synchrotron emission is seen) will be a question of future investigation.

4 Summary

External interaction such as intracluster winds can work together with dynamo action providing an additional agent amplifying the magnetic field in spiral galaxies. Such an interaction can remain imprinted in the magnetic field configuration, producing e.g. depolarized channels not connected to any underlying optical structure as well as polarized (magnetic) arms not coinciding with optical ones. Vertical gas flows form the vertical magnetic field structure, resembling (and amplifying) the poloidal field component resulting from dynamo action.

In our experiment only the regular magnetic field component is calculated. For comparison with total power maps the random magnetic field component has to be introduced in our model.

References

Beck R. (2000) *Phil. Trans. R. Soc. Lond. A* **358**, 777.
Beck R., Brandenburg A., Moss D., Shukurov A., Sokoloff D. (1966) *Annnu. Rev. Astron. Astrophys.* **34**, 155.
Chyży K.T., Urbanik M., Soida M., Beck R. (2002) *Astrophys. and Space Science* **281**, 409.
Chyży K.T., Beck R., Urbanik M. (2003) *Astron. Astrophys.*, submitted.
Isaaks E.H., Srivastava R. (1989) *An Introduction to Applied Geostatistics*, Oxford University Press, Chapter 12.
Otmianowska-Mazur K., Vollmer B. (2003) *Astron. Astrophys.* **402**, 879.
Soida M., Urbanik M., Beck R. (1996) *Astron. Astrophys.* **312**, 409.
Soida M., Urbanik M., Beck R., Wielebinski R. (1999) *Astron. Astrophys.* **345**, 461.
Soida M., Urbanik M., Beck R., Wielebinski R., Balkowski C. (2001) *Astron. Astrophys.* **378**, 40.
Stone J.M., Norman M.L. (1992) *Astrophys. J. Suppl.* **80**, 791.
Vollmer B., Cayatte V., Balkowski C., Duschl W.J. (2001) *Astrophys. J.* **561**, 708.